JOURNAL OF SOLID STATE CHEMISTRY

Volume 178, Number 11, November 2005

CONTENTS

Regular Articles

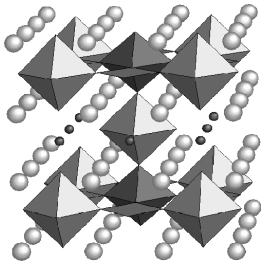

Schematic representation of the structure of tetragonal $Ba_4CaCu_3O_{8+\delta}$. Cu atoms and CuO_z coordination polyhedra: dark grey; CaO_6 octahedra and Ba atoms: light grey.

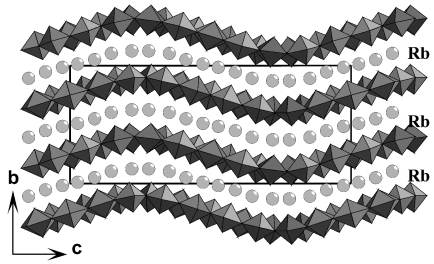

Puckered layered structure of $Rb_8U_9O_{31}$.

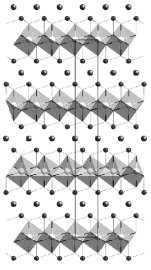

Structure of $CeAuAl_4Ge_2$ viewed down the [010] direction.

Regular Articles—Continued

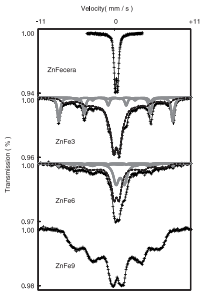

Mössbauer spectra of $ZnFe_2O_4$ ceramic and ball-milled ZnO–α-Fe_2O_3 mixture. Grey curves: contribution of α-Fe_2O_3, α-Fe or FeO. Dashed black curves: contribution of spinel phase.

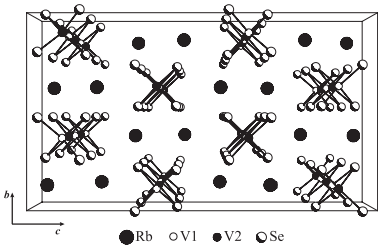

Unit cell of $RbVSe_2$ viewed down [100].

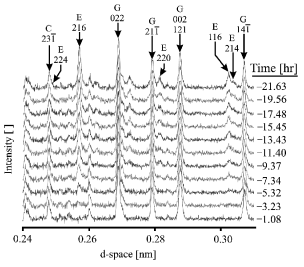

Time evolution of the $+145^\circ$ SEPD detector diffraction data for the hydration at 50 °C. Prominent reflections are indicated for tricalcium aluminate (C), ettringite (E), and gypsum (G).

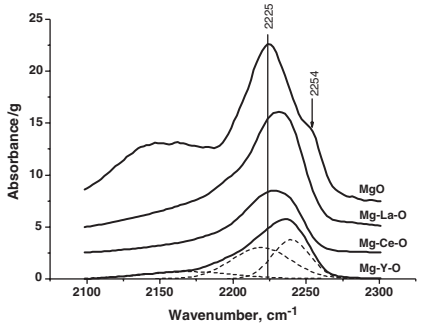

FTIR spectra of $CDCl_3$ adsorbed on MgO and binary Mg–*M*–O (≈5 mol% M_2O_3) systems at 0 °C.

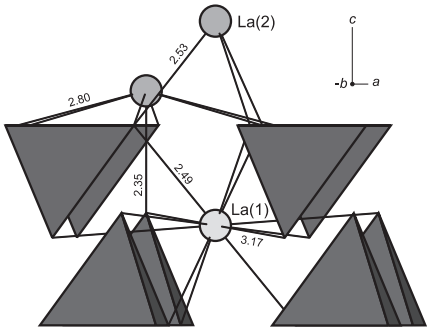

Ideal structure of barium phosphate-type $La_{2.67}(SiO_4)_2$.

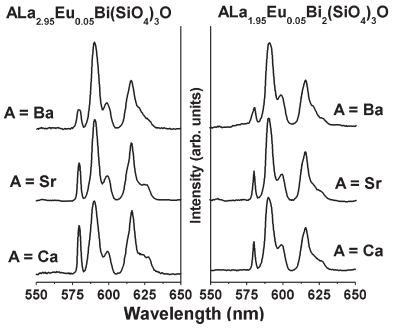

Photoluminescence emission spectra of Eu^{3+} in $A La_3Bi(SiO_4)_3O$ and $A La_2Bi_2(SiO_4)_3O$ [*A* = Ca, Sr and Ba]; $\lambda_{exc} = 395$ nm.

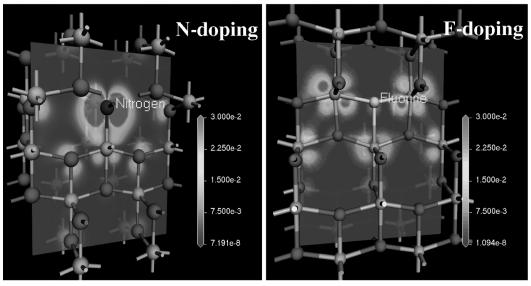

Electron density maps of the N-doped and F-doped TiO_2.

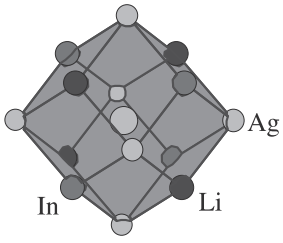

Heusler-type structure of $LiAg_2In$. First and second coordination polyhedron for a central Ag-atom.

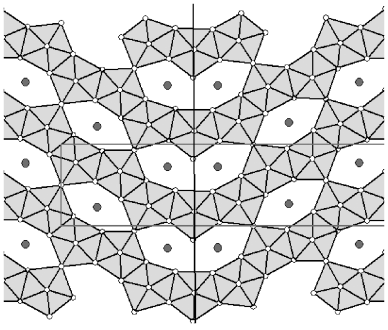

Schematic of structural basis for L-Ta_2O_5-related phases.

Continued

Synthesis and characterization of a Ruddlesden–Popper compound: Sr_3FeMoO_7

Zhaofei Li, Guobao Li, Junliang Sun, Liping You, Chun-K. Loong, Yingxia Wang, Fuhui Liao and Jianhua Lin

Page 3315

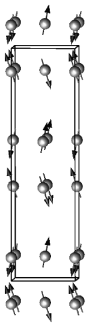

The magnetic structure of Sr_3FeMoO_7 was determined through neutron diffraction at 10 K. It was refined with an antiferromagnetic model in the magnetic space group An' with the cell parameters $a = 5.5561(3)$ Å and $c = 20.430(2)$ Å. The *B*-site atoms split into two independent atoms, which are antiferromagnetically coupled with almost the same magnetic moment $\mu_{M1} = 1.82(1)\mu_B$ and $\mu_{M2} = 1.68(1)\mu_B$.

$Ce_{10}[Si_{10}O_9N_{17}]Br$, $Nd_{10}[Si_{10}O_9N_{17}]Br$ and $Nd_{10}[Si_{10}O_9N_{17}]Cl$ oxonitridosilicate halides with a new layered structure type

Alexandra Lieb and Wolfgang Schnick

Page 3323

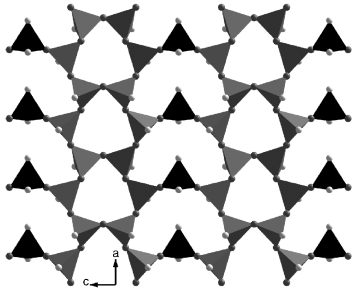

The novel oxonitridosilicate layers are made up of condensed $[Si(O,N)_4]$ tetrahedra of Q^2 and Q^3 type, thus forming six- and eight-membered tetrahedra rings.

Syntheses, crystal structures and luminescent properties of two new 1D d^{10} coordination polymers constructed from 2,2′-bibenzimidazole and 1,4-benzenedicarboxylate

Lili Wen, Yizhi Li, Dongbin Dang, Zhengfang Tian, Zhaoping Ni and Qingjin Meng

Page 3336

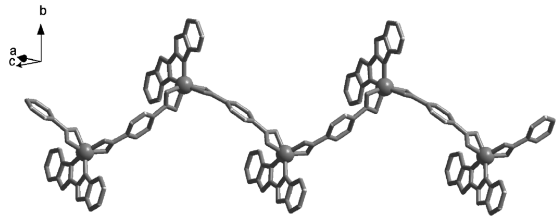

The crystal structures, TG and photoluminescence properties on two new d^{10} one-dimensional coordination polymer $[Zn(H_2bibzim)(BDC)]_n$ (**1**) and $[Cd(H_2bibzim)(BDC)]_n$ (**2**) have been reported.

Solvothermal synthesis of new metal organic framework structures in the zinc–terephthalic acid–dimethyl formamide system

Henrik Fanø Clausen, Rasmus Damgaard Poulsen, Andrew D. Bond, Marie-Agnes S. Chevallier and Bo Brummerstedt Iversen

Page 3342

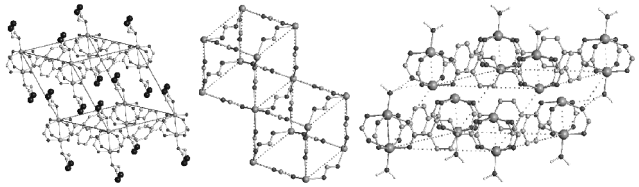

Three different metal organic framework structures with similar crystal habits are obtained from the same solvothermal synthesis batch.

S-, N- and C-doped titanium dioxide nanoparticles: Synthesis, characterization and redox charge transfer study

K. Madhusudan Reddy, Babita Baruwati, M. Jayalakshmi, M. Mohan Rao and Sunkara V Manorama

Page 3352

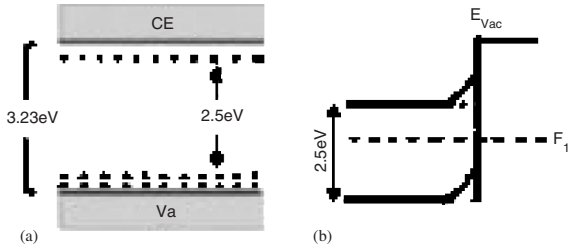

Schematic representations of N-doped TiO_2: (a) band diagram and (b) band bending at the interface.

Two-dimensional metal-organic framework constructed from 4,4′-bipydine and 1,2,4-benzenetricarboxylate: Synthesis, structure and magnetic properties

Lei Wang, Ming Yang, Zhan Shi, Yan Chen and Shouhua Feng

Page 3359

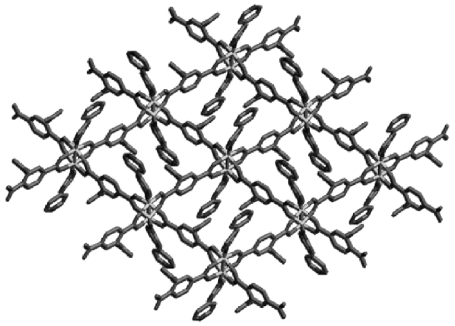

View of the structure of **2** along the *c*-axis.

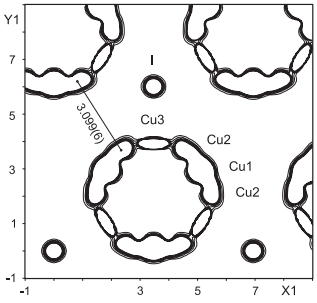

Pseudo-cluster of copper in high temperature phase of Cu_6PS_5I.

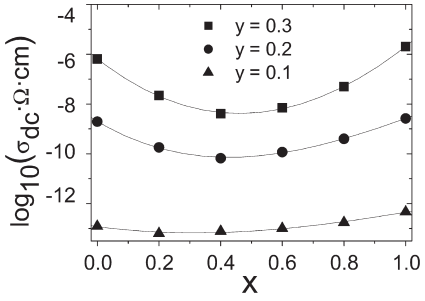

Composition-dependent dc conductivity of glassy y $[xLi_2O\cdot(1-x)Na_2O]\cdot(1-y)B_2O_3$ ($x = 0$, 0.2, 0.4, 0.6, 0.8, 1.0, and $y = 0.1$, 0.2, 0.3) at 473 K.

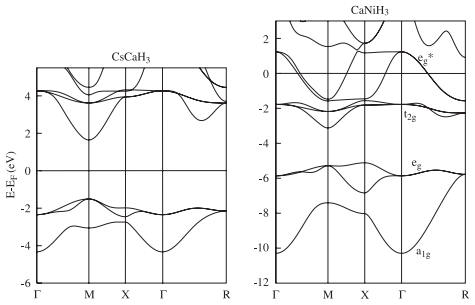

Band structure of $CsCaH_3$. Band structure of $CaNiH_3$ at the theoretical equilibrium volume.

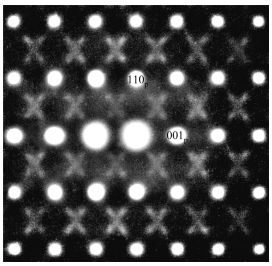

Shows a typical $\langle 110\rangle_p$ zone axis EDP of the nominally Mn^{2+}/Nb^{5+} disordered, metrically cubic of $Ba_3MnNb_2O_9$. Notice the presence of diffuse crosses implying the presence of $\{111\}_p$ stacking fault and rotational twin disorder.

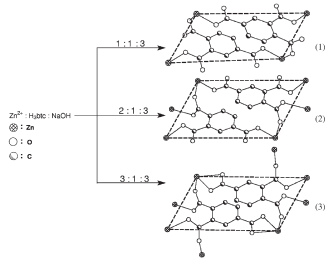

The relations of molar ratios of the reactants and structures with coordination mode of btc^{3-} ligand.

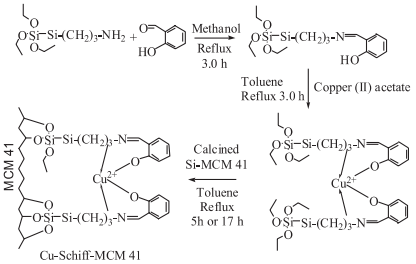

Synthesis of the Cu–Schiff MCM 41 material covalently anchored onto the Si-MCM 41 surface by the esterification of siloxane groups from copper–Schiff base complex and surface silanol groups of Si-MCM 41.

Continued

Directing the structures of silver-antimony sulphides: A new topological variant of the $[Ag_5Sb_3S_8]^{2-}$ double layer
Anthony V. Powell, Jürgen Thun and Ann M. Chippindale
Page 3414

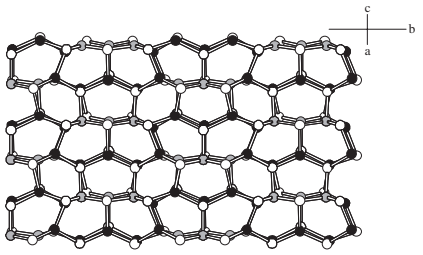

View along the [1 0 1] direction of an $[Ag_5Sb_3S_8]^{2-}$ double layer in $[C_6H_{20}N_4][Ag_5Sb_3S_8]$ formed from linkage through Ag–S bonds of a pair of crystallographically equivalent honeycomb-like sheets of fused six-membered silver–antimony sulphide rings.

Ternary lithium stannides $Li_xT_3Sn_{7-x}$ (T = Rh, Ir)
Puravankara Sreeraj, Daniel Kurowski, Rolf-Dieter Hoffmann, Zhiyun Wu and Rainer Pöttgen
Page 3420

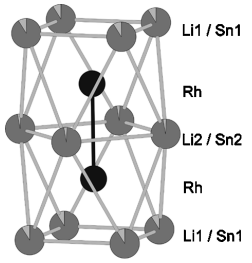

The monomeric building unit in the cubic crystal structure of $Li_xT_3Sn_{7-x}$ (T = Rh, Ir). The transition metal and tin atoms are drawn as black and light gray circles, respectively. The sectors of the tin sites correspond to the different lithium content.

The role of Mn in the electronic structure of $Ba_3Ti_2MnO_9$
G. Radtke, C. Maunders, S. Lazar, F.M.F. de Groot, J. Etheridge and G.A. Botton
Page 3426

Magnetic and transport properties of high-pressure synthesized perovskite cobalt oxide $(Sr_{1-x}Ca_x)CoO_3$ ($0 \leqslant x \leqslant 0.8$)
S. Balamurugan, M. Xu and E. Takayama-Muromachi
Page 3431

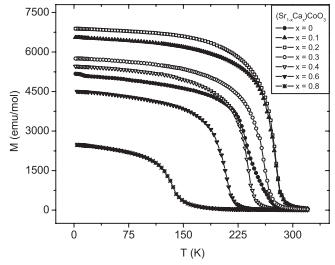

Temperature dependence of the dc-magnetization M of the $(Sr_{1-x}Ca_x)CoO_3$ system measured at an applied field of 1 kOe by the field cooling mode.

Hydrothermal synthesis and crystal structures of new uranyl oxalate hydroxides: α- and β-$[(UO_2)_2(C_2O_4)(OH)_2(H_2O)_2]$ and $[(UO_2)_2(C_2O_4)(OH)_2(H_2O)_2]\cdot H_2O$
Laurence Duvieubourg, Guy Nowogrocki, Francis Abraham and Stéphane Grandjean
Page 3437

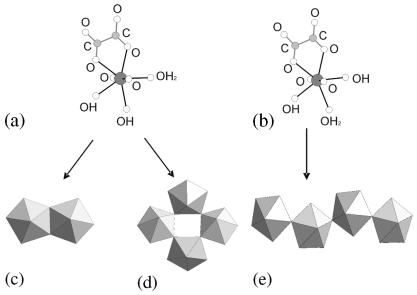

The two configurations of the U-centered pentagonal bi-pyramid and the structural polyhedral building units in the three $[(UO_2)_2(C_2O_4)(OH)_2(H_2O)_2]$ networks.

Structures and syntheses of four Np^{5+} sulfate chain structures: Divergence from U^{6+} crystal chemistry
Tori Z. Forbes and Peter C. Burns
Page 3445

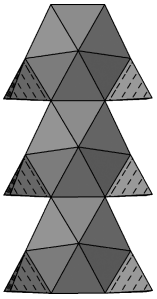

The chain of neptunyl bipyramids and sulfate tetrahedra.

Synthesis, structure, and magnetic properties of $SrMn_{1-x}Ga_xO_{3-\delta}$ (x = 0–0.5) perovskites
B. Dabrowski, E.N. Caspi, S. Kolesnik, O. Chmaissem, J. Mais and J.D. Jorgensen
Page 3453

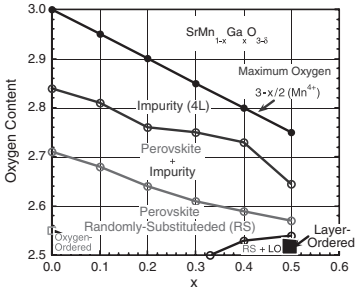

Summary of characteristic oxygen contents that define stability ranges of the single-phase and multi-phase $SrMn_{1-x}Ga_xO_{3-\delta}$ perovskites with randomly substituted (RS) and layer-ordered (LO) B-site cations.

Long-range magnetic ordering of quasi-one-dimensional $S=1/2$ Heisenberg antiferromagnet $Sr_2Cu(PO_4)_2$
Alexei A. Belik, Shinya Uji, Taichi Terashima and Eiji Takayama-Muromachi
Page 3461

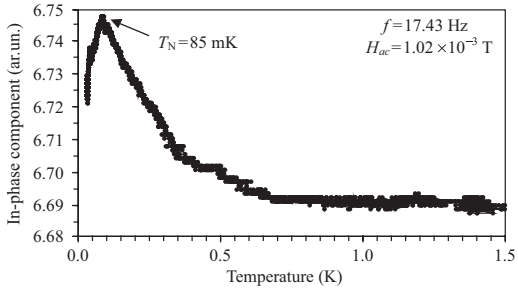

Temperature dependence of the in-phase component of the AC susceptibility between 0.03 and 1.5 K in $Sr_2Cu(PO_4)_2$.

Hole doping and superconductivity characteristics of the $s=1$, 2 and 3 members of the (Cu,Mo)-12s2 homologous series of layered copper oxides
M. Karppinen, Y. Morita, T. Kobayashi, I. Grigoraviciute, J.M. Chen, R.S. Liu and H. Yamauchi
Page 3464

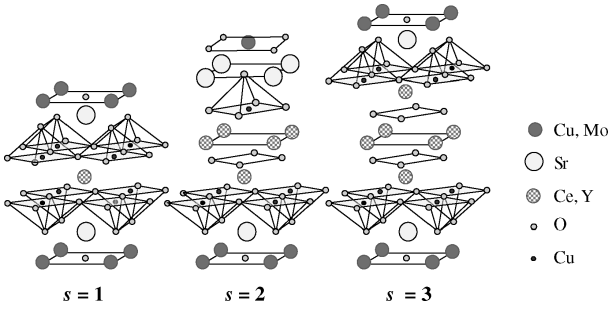

Crystal structures of the first three members of the (Cu,Mo)-12s2 homologous series of superconductive copper oxides.

The crystal structure of $CuSb_2O_3Br$: Slabs from cubic Sb_2O_3 interspersed between puckered hexagonal CuBr-type layers
Zuzana Mayerová, Mats Johnsson and Sven Lidin
Page 3471

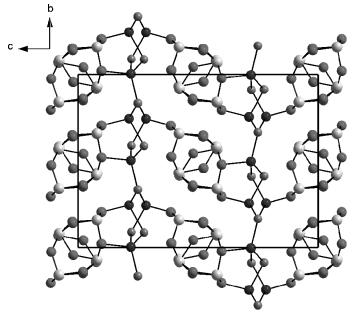

The compound $CuSb_2O_3Br$ is described. The layers consist of Sb_4O_6 cages resembling those in cubic Sb_2O_3 interspersed between puckered CuBr layers that bear similarities to the layers in hexagonal CuBr. Cu–O bonds link the Sb_4O_6 cages with CuBr.

Phase relationships in the pseudo-binary 2(ZnTe)-$CuInTe_2$ system
Liudmila Roussak, Gerald Wagner, Susan Schorr and Klaus Bente
Page 3476

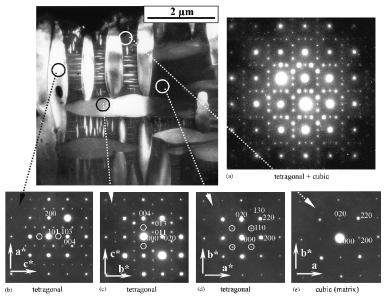

TEM dark-field image and SAD patterns of differently oriented tetragonal domains (b–d) and cubic matrix (e). The compositions of the domains and matrix are $Zn_{0.123}Cu_{0.402}In_{0.475}Te$ and $Zn_{0.279}Cu_{0.313}In_{0.407}Te$, respectively. The SAD pattern taken from the multi-domain region (a) is a superposition of all patterns (b–e). Beam direction (bd) close to [001]. The encircled spots in (b–d) are caused by a stannite-type cation ordering.

A magnetic organic–inorganic composite: Synthesis and characterization of magnetic 5-aminosalicylic acid intercalated layered double hydroxides
Hui Zhang, Kang Zou, Hui Sun and Xue Duan
Page 3485

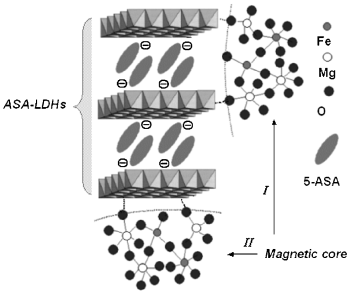

A schematic structural model of nanosized magnetic organic–inorganic hybrid composite involving 5-aminosalicylic acid intercalated layered double hydroxides coated on a ferrite core.

Synthesis and characterization of $K(In_{6.5}Ag_{6.5})$
Mark S. Bailey, Michael A. McGuire and Francis J. DiSalvo
Page 3494

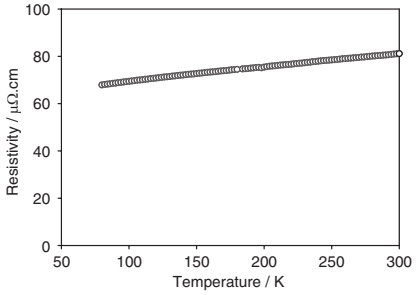

The measured electrical resistivity of a single crystal of $K(In_{6.5}Ag_{6.5})$.

Continued

Preparation and photocatalytic activity of $ZnO/TiO_2/SnO_2$ mixture

Cun Wang, Bo-Qing Xu, Xinming Wang and Jincai Zhao

Page 3500

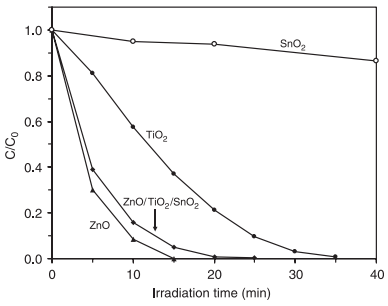

Comparison of the photocatalytic activities of ZnO, TiO_2, SnO_2 and $ZnO/TiO_2/SnO_2$ after the calcination at 500 °C for 2 h. Loading of the photocatalysts: 2.5 g/L; concentration of methyl orange: 20 mg/L.

Synthesis of Sm^{3+}-doped strontium barium niobate crystals in glass by samarium atom heat processing

Nakorn Chayapiwut, Tsuyoshi Honma, Yasuhiko Benino, Takumi Fujiwara and Takayuki Komatsu

Page 3507

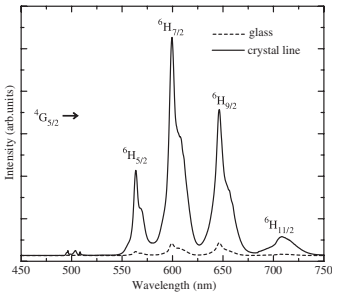

This figure is the micro-photoluminescence spectra for the glass part and crystal line written by YAG laser irradiation in $10Sm_2O_3 \cdot 40SBN \cdot 50B_2O_3$ glass. We propose from these spectra that Sm^{3+} ions are incorporated into SBN crystals.

New metal phosphonates containing coordination piperazine or pyridyl groups

Jun-Ling Song and Jiang-Gao Mao

Page 3514

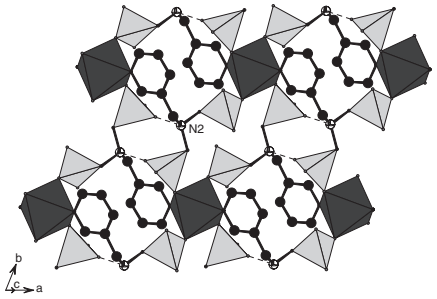

A (001) 2D metal phosphonate layer in **2**. The CoN_2O_4 octahedra and C–PO_3 tetrahedra are shaded in dark and light gray, respectively. C and N atoms are drawn as black and octanded circles, respectively. Hydrogen bonds are represented by dashed lines.

The synthesis of ZnS hollow nanospheres with nanoporous shell

Hua-Feng Shao, Xue-Feng Qian and Zi-Kang Zhu

Page 3522

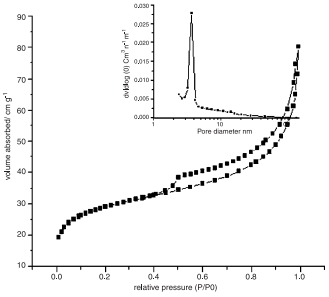

Nitrogen adsorption/desorption isotherm and Brunauer–Emmett–Teller (BET) pore-size distribution plot (inset) of ZnS hollow spheres.

Syntheses and crystal structures of several novel alkylammonium iodobismuthate materials containing the 1,3-bis-(4-piperidinium)propane cation

Andrea M. Goforth, LeRoy Peterson Jr., Mark D. Smith and Hans-Conrad zur Loye

Page 3529

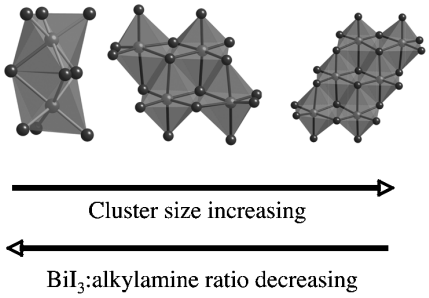

The syntheses and single-crystal X-ray structures of five new inorganic–organic compounds containing the alkylammonium cation 1,3-bis-(4-piperidinium)propane in addition to a complex iodobismuthate anion are presented and discussed. In general, structures having larger anions are produced from greater relative ratios of the inorganic starting material to the organic starting material.

Preparation and thermal expansion of $\left(M^{III}_{0.5}M'^{V}_{0.5}\right)P_2O_7$ with the cubic ZrP_2O_7 structure

Tamas Varga, Angus P. Wilkinson, Michael S. Haluska and E. Andrew Payzant

Page 3541

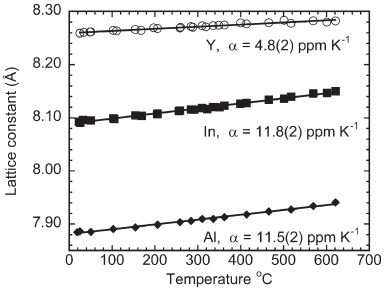

The average linear coefficient of thermal expansion (~25–600 °C) for $M^{III}_{0.5}(Nb/Ta)_{0.5}P_2O_7$ decreases dramatically on going from In to Y. The behavior of the Y compound is similar to that of ZrP_2O_7 at high temperatures (>290 °C), whereas the In compound is similar to ZrP_2O_7 at low temperature.

A comparison of the structure and localized magnetism in Ce_2PdGa_{12} with the heavy fermion $CePdGa_6$

Robin T. Macaluso, Jasmine N. Millican, Satoru Nakatsuji, Han-Oh Lee, B. Carter, Nelson O. Moreno, Zachary Fisk and Julia Y. Chan

Page 3547

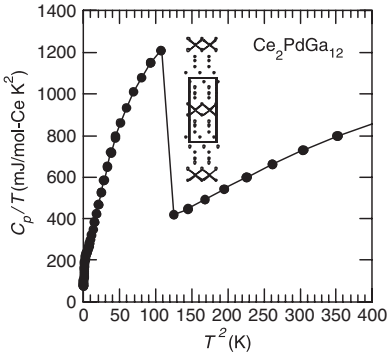

The C_P/T vs. T^2 plot is shown. The sudden jump in the specific heat at $T^2 \sim 120$ K corresponds to the magnetic transition at $T_N = 11$ K observed in magnetic susceptibility data. After fitting the data to $C_P = \gamma T + \alpha T^3$, the electronic contribution to the specific heat, γ, is equal to 72 mJ/mol K^2. Thus Ce_2PdGa_{12} is not a likely candidate for heavy fermion behavior. The structure of Ce_2PdGa_{12} is compared to the closely related structure of $CePdGa_6$, which is a heavy fermion compound with $\gamma \sim 230$ mJ/mol K^2. The structure of Ce_2PdGa_{12} is shown as the inset where Ce, Pd, and Ga are shown as black, gray, and white circles, respectively. The unit cell is shown as a solid line.

Two new two-dimensional organically templated phosphite compounds: $(C_6H_{16}N_2)_{0.5}[M(HPO_3)F]$, M = Fe(II) and Co(II): Solvothermal synthesis, crystal structures, thermal, spectroscopic, and magnetic properties

Sergio Fernández-Armas, José L. Mesa, José L. Pizarro, U-Chan Chung, María I. Arriortua and Teófilo Rojo

Page 3554

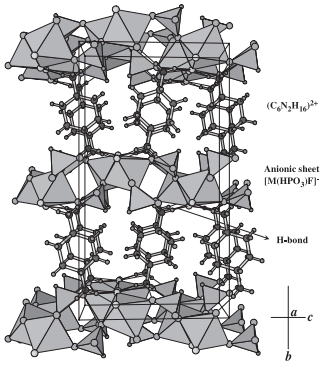

Polyhedral view of the layered crystal structure for the isostructural $(C_6H_{16}N_2)_{0.5}[M(HPO_3)F]$ (M = Fe and Co) compounds.

Synthesis, crystal structure and two-dimensional infrared correlation spectroscopy of a layer-like transition metal (TM)-oxalate templated polyoxovanadium borate

Yanning Cao, Hanhui Zhang, Changcang Huang, Qiyu Yang, Yiping Chen, Ruiqing Sun, Fengli Zhang and Wenjun Guo

Page 3563

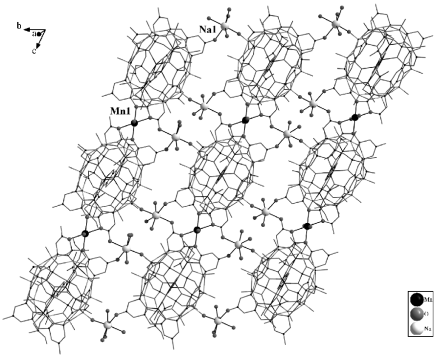

Wires representation of the 2D layer structure constructed from $V_{10}B_{28}$ clusters and the octahedral Mn(II) and Na^+ sites in ball-and-stick representation. The dissociated water and en molecules between the clusters are omitted for clarity.

Acid and redox properties of mixed oxides prepared by calcination of chromate-containing layered double hydroxides

M. del Arco, D. Carriazo, C. Martín, A.M. Pérez-Grueso and V. Rives

Page 3571

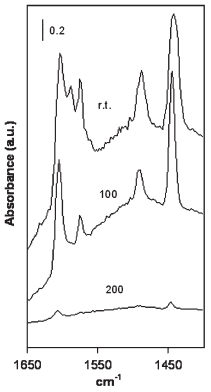

Layered double hydroxides with intercalated chromate have been prepared and characterised; the surface acidity properties of the calcined products have been studied.

Continued

Synthesis, crystal structure and vibrational spectra characterization of $M^{I}La(PO_3)_4$ (M^{I} = Na, Ag)
Mohamed El Masloumi, Inhar Imaz, Jean-Pierre Chaminade, Jean-Jacques Videau, Michel Couzi, Mohamed Mesnaoui and Mohamed Maazaz
Page 3581

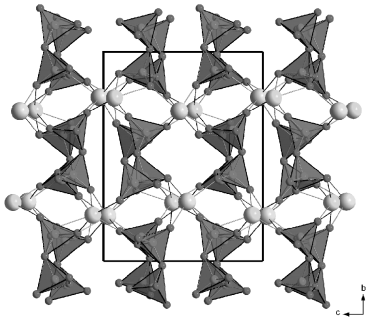

Projection in *bc* plane of the $M^{I}La(PO_3)_4$ structure (M^{I} = Na, Ag).

Independent structural and valence state transitions in the cation-ordered double perovskites $Ba_{2-x}Sr_xTbIrO_6$
Qingdi Zhou and Brendan J. Kennedy
Page 3589

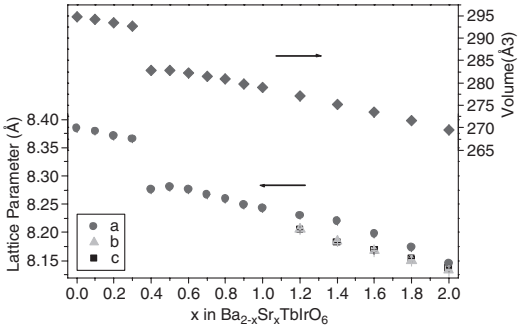

Composition dependence of the lattice parameters and volumes in the series $Ba_{2-x}Sr_xTbIrO_6$. For ease of comparison the value for the *a* and *b*-parameters in the monoclinic phase have been scaled by $2^{0.5}$.

Rapid Communications

Simultaneous deposition of Ni nanoparticles and wires on a tubular halloysite template: A novel metallized ceramic microstructure
Yubin Fu and Lide Zhang
Page 3595

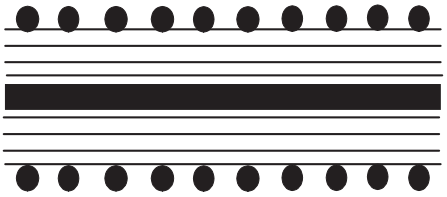

A novel metallized ceramic microstructure formed with Ni nanoparticles on the outer surface and wires simultaneously in the lumen site of tubular halloysite template.

Synthesis of crystalline yttrium oxycarbonate in a single phase
Nobuhito Imanaka, Toshiyuki Masui, Yuhei Mayama and Kazuhiko Koyabu
Page 3601

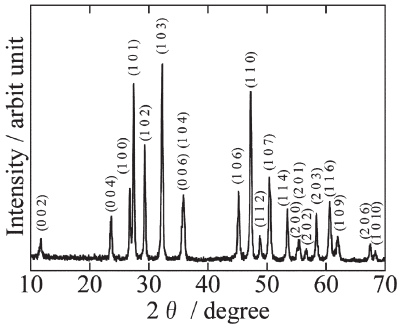

Crystalline yttrium oxycarbonate was synthesized in a single phase form for the first time by a flux method using the $0.476Li_2CO_3$–$0.270Na_2CO_3$–$0.254K_2CO_3$ eutectic mixture.

NOTICE

The Keyword Index for Volume 178 will appear in the December 2005 issue as part of a cumulative index for the year 2005.